Journal of Nuclear Medicine, published on February 23, 2017 as doi:10.2967/jnumed.116.182790

Association between osteogenesis and inflammation during the progression of calcified plaques as evaluated by combined ^{18}F-NaF and ^{18}F-FDG PET/CT

Running Title: NaF and FDG during plaque progression

Xiang Li[1*], Daniel Heber[1*], Jacobo Cal Gonzalez[2], Georgios Karanikas[1], Marius E. Mayerhoefer[3], Sazan Rasul[1], Dietrich Beitzke[4], Xiaoli Zhang[5], Hermine Agis[6], Markus Mitterhauser[1], Wolfgang Wadsak[1], Thomas Beyer[2], Christian Loewe[4], Marcus Hacker[1**]

* Xiang Li and Daniel Heber contributed equally to this work

** Corresponding author

1. Division of Nuclear Medicine, Department of Biomedical Imaging and Image-guided Therapy, Medical University of Vienna, Vienna, Austria

2. Center for Medical Physics and Biomedical Engineering, General Hospital Vienna, Medical University of Vienna. Vienna, Austria

3. Division of General and Pediatric Radiology, Department of Biomedical Imaging and Image-guided Therapy, Medical University of Vienna, Vienna, Austria

4. Division of Cardiovascular and Interventional Radiology, Department of Biomedical Imaging and Image-guided Therapy, Medical University of Vienna, Vienna, Austria

5. Department of Nuclear Medicine, Beijing Anzhen Hospital, Capital Medical University, Beijing, China

6. Department of Medicine I, Clinical Division of Hematology and Hemostaseology, Medical University of Vienna, Vienna, Austria

Word Count: 4735

Corresponding Author:

Marcus Hacker, M.D.

Marcus.hacker@meduniwien.ac.at

First Author:

Xiang Li, Ph.D.

Xiang.Li@meduniwien.ac.at

Both authors: Division of Nuclear Medicine, Department of Biomedical Imaging and Image-guided Therapy, Medical University of Vienna, Austria

Währinger Gürtel 18-20, 1090 Vienna, Austria

ABSTRACT:

^{18}F-fluorodeoxyglucose (^{18}F-FDG) is the most widely validated positron emission tomography (PET) tracer for the evaluation of atherosclerotic inflammation. ^{18}F-sodium fluoride (^{18}F-NaF) has also been recently considered a potential novel biomarker of osteogenesis in atherosclerosis. We aimed to analyze the association between inflammation and osteogenesis at different stages of atherosclerosis, as well as the interrelationship between these two processes during disease progression. **Methods:** Thirty-four myeloma patients underwent ^{18}F-NaF and ^{18}F-FDG PET/computed tomography (CT) examinations. Three groups (non-calcified; mildly calcified; and severely calcified lesions) were divided based on the calcium density as measured in Hounsfield units (HU) by CT. Tissue-to-background ratios (TBR) were determined from PET for both tracers. The association between inflammation and the osteogenesis during atherosclerosis progression was evaluated in 19 patients who had at least two examinations with both tracers. **Results**: There were significant correlations between the TBR_{max} values of the two tracers (Spearman's r=0.5, p<0.01, Pearson r=0.4, p<0.01) in the 221 lesions at baseline. In non-calcified lesions, highest uptake of both tracers was observed, but without any correlation between both tracers (Pearson r=0.06, p=0.76). Compared to non-calcified plaques, concordant significantly lower accumulation was found in mildly calcified plaques, with good correlation between the tracers (Pearson r=0.7, p<0.01). In addition, there was enhanced osteogenesis-derived ^{18}F-NaF uptake, and regressive inflammation-derived ^{18}F-FDG uptake in severely calcified lesions (Pearson r=0.4, p<0.01). During follow-up, there was an increased calcium density and an increased mean ^{18}F-NaF uptake observed, while the mean ^{18}F-FDG uptake decreased. The majority of non-calcified (86%) and mildly calcified (81%) lesions and 47% of severely calcified lesions had a concordant development of both vascular inflammation and osteogenesis. **Conclusion:** The combination of ^{18}F-NaF and ^{18}F-FDG PET imaging promotes an understanding of the mechanism of plaque progression, thereby providing new insights into plaque stabilization.

Keywords: Atherosclerosis, calcification, inflammation, PET/CT, ^{18}F-FDG, ^{18}F-NaF

INTRODUCTION

The histopathological characteristics of vulnerable plaques include spotty calcification, a thin fibrous cap, a large necrotic core, and intraplaque hemorrhage (*1*). Among these, the continuous accumulation of macrophages can be found in all developmental stages of atherosclerotic arteries, which contributes to plaque instability (*2*). Thus, vascular inflammation, including macrophage density, infiltration, differentiation, and apoptosis rate, is recognized as a prominent predictor of a vulnerable lesion (*3*). Moreover, as a common complication in atherosclerosis, vascular calcifications in atherosclerotic patients are more progressive, extensive, and severe compared to those in the non-atherosclerotic population, due to enhanced mineral metabolism during the formation of a plaque, which involves intensive osteogenic activity and increased volume (*4*).

Macrophage infiltration and endothelial activation trigger osteogenesis, which initiate atherosclerosis; and subsequently, osteogenic activity and calcium density are closely associated with macrophage accumulation (*5*). If inflammation continues, it has often been observed that thin-cap, inflamed fibroatheromas with high vulnerability include spotty calcium deposits, which may serve as an independent predictor of increased vulnerability (*6*). Another prominent view is that decreased osteogenic activity is coupled with a reduction of inflammation that drives the disease to the advanced end-stage of atherosclerosis. In advanced stages, the presence of intensive calcifications with limited inflammation might serve as a stabilizer in fibrous atherosclerotic lesions (*4,6,7*).

CT quantification of vascular calcification has been extensively validated and the Hounsfield units (HU) from unenhanced low-dose CT scans were shown to be associated with the extent of calcified atherosclerotic lesions (*8*), but there is a lack of characterization of early osteogenic activity. Recently, it was discovered that atherosclerotic calcium is histomorphologically indistinguishable from bone, and the formation of vascular calcium is similar to bone development and metabolism. Thus, it was proposed that osteogenesis could be a marker for atherosclerotic disease (*9*). ^{18}F-NaF has been used as a bone PET tracer to define osteogenic activity, and the feasibility of ^{18}F-NaF PET/CT to identify increased intra-plaque osteogenic activity in vivo was

confirmed in the context of atherosclerotic plaque imaging (*10-13*). This process is dependent on the density of hydroxyapatite, as well as the exposed surface of calcification in vasculature. In addition, ^{18}F-FDG is trapped intracellularly after phosphorylation by hexokinase to allow intra-tissue glucose metabolism assessment. It is also the most widely validated PET tracer to evaluate inflammation within the atherosclerotic plaque based on the glucose metabolism of macrophages (*2*). There are published studies that have also evaluated the association between arterial calcification and the inflammation of vascular disease, and demonstrated macrophage/monocyte regulation of vascular calcification through the induction of osteoblastic differentiation and mineralization during the progression of atherosclerosis (*14,15*). In the present study, we investigated the arterial uptake of ^{18}F-NaF and ^{18}F-FDG and aimed to analyze the association between tracer accumulation and calcium density at different stages of atherosclerosis. Second, we aimed to examine the inter-relationship between inflammation and osteogenesis during plaque growth.

MATERIALS AND METHODS

Patient Population

Thirty-four myeloma patients were included in this retrospective study. They underwent both ^{18}F-NaF PET/CT to detect the presence of bone metastases and ^{18}F-FDG PET/CT for staging or restaging purposes within three days. Relevant baseline characteristics of the patients are reported in Table 1. Nineteen patients were scheduled for follow-up scans with both ^{18}F-NaF and ^{18}F-FDG PET/CT at 15 ± 4 months after baseline, eleven of them underwent a second follow-up scans with both tracers 12 ± 6 months later. These scans were used to characterize osteogenesis and inflammation during plaque progression. Patients with history of systemic inflammatory disease, statin/ezetimibe/PCSK9 medication use and clinical cardiovascular events of myocardial infarction or stroke between baseline and follow-up scans were excluded. The clinical institutional review board approved this study and patients gave written informed consent.

Radiotracer preparation

Both ^{18}F-FDG and ^{18}F-NaF were produced using the fully automated FASTlab platform (GE Healthcare) with GMP compliant single-use cassettes under aseptic conditions in concordance with national health legislature without any objections by the local health authorities. Full radiopharmaceutical quality control as described in the European Pharmacopoeia's specific monographs were completed before release of the product for in-vivo application. Radiotracer preparations were performed once a day regardless of the patient numbers.

PET/CT Imaging

All patients were imaged on a hybrid PET/CT system (Siemens Biograph TPTV 64, Siemens, USA). Patients fasted for at least six hours before tracer injection (Serum glucose level at baseline was 104±21mg/dL). Patients received ^{18}F−NaF (310-380) MBq and ^{18}F-FDG (300-450) MBq within 3 days. Transmission data was acquired using a low-dose CT (^{18}F−NaF) and a contrast-enhanced CT (^{18}F-FDG). PET images were acquired by using two min per bed position and reconstructed with an iterative algorithm with Point Spread Function correction (*16*), including all relevant data corrections. 4 iterations and 21 subsects were used in the reconstruction.

Image Analysis

For each patient, eight segments of the large arteries were assessed: the left and right carotid arteries; the ascending thoracic aorta; the aortic arch; the descending thoracic aorta; the abdominal aorta; and the left and right iliac arteries. As a first step, non-contrast CT images were visually evaluated for the presence of calcified plaques in the eight arterial segments. The presence of vascular calcifications was defined as a luminal area with a minimum calcium density of 130 HU by regions of interest measurement (*17*). In the present study, three groups of lesions were defined for vascular calcification: group 1, non-calcified lesions: calcium density <130 HU; group 2, mildly calcified lesions: calcium density 130≤HU≤399; group 3, severely calcified lesions: calcium density ≥ 400 HU.

^{18}F-NaF and ^{18}F-FDG uptake in the calcified lesions was assessed with commercially available software (Hermes Hybrid 3D, Hermes Medical Solutions, Stockholm, Sweden). The maximum standardized uptake value values of both ^{18}F-FDG and ^{18}F-NaF uptake at all atherosclerotic lesions were determined by regions of interest measurements. To calculate tissue-to-background ratios (TBR), Standardized uptake value values were corrected for background blood-pool activity, which was calculated as the mean uptake from three regions of interests within the lumen of veins (*18,19*). The mean TBR_{max} of the uptake was calculated for both tracers. For analyses of follow-up scans, the same lesions that were detected on the baseline scans were considered for both tracers. In order to evaluate the relationship between the uptake ratios of the two tracers, we performed linear regression analyses of baseline TBR_{max} (^{18}F-NaF) and TBR_{max} (^{18}F-FDG) in the three groups individually.

We used a predefined threshold TBR (^{18}F-FDG) value of 1.6 to identify increased inflammation (*20,21*), and self-defined threshold TBR (^{18}F-NaF) of 1.8 to indicate positive osteogenesis. Relevant calcium density changes were estimated as well. Stabilized/retarded development and progressive/positive development of the two processes is detailed in Table 2. The interaction between atherosclerotic inflammation, osteogenesis, and subsequent calcification evolution was assessed.

Statistical Analysis

Apart from descriptive statistics at baseline, comparisons among the three groups of lesions were performed using one-way analysis of variance test. Games-Howell post-hoc test was performed to confirm where the differences occurred. In progression assessment, paired T-test was performed to assess differences of uptake ratios in all lesions over time as well as for anti-tumor medication assessment. The rank correlations of maximum TBR value of ^{18}F-NaF and ^{18}F-FDG in the arteries were assessed using the Spearman correlation. Associations between progressive calcium scores on CT with baseline and progressive uptake data on PET were assessed using Pearson linear regression analysis. P-values ≤0.05 were considered statistically

significant.

RESULTS

Osteogenesis and macrophage metabolism in relation to plaque calcification

At baseline, 221 atherosclerotic lesions (26 non-calcified and 195 calcified lesions) were detected within the eight arterial segments of the 34 patients. The mean TBR_{max} of ^{18}F-NaF uptake was significantly higher than that of the ^{18}F-FDG uptake (2.4±0.8 vs.1.8±0.5; p <0.01). The uptake of both tracers correlated significantly, but with low Spearman's rank correlation coefficient (r=0.5, p<0.01). In addition, a linear correlation coefficient of 0.4 (p<0.01) between the TBR_{max} values of the two tracers was calculated by the Pearson correlation method for all lesions (Fig.1), where the highest degree of correlation was shown for the group of mildly calcified (r=0.7, p<0.01), followed by severely calcified lesions (r=0.4, p<0.01). There was no correlation between the two tracers found for non-calcified lesions (r=0.06, p=0.76) (Fig. 1). In the group analyses at baseline, significantly increased uptake ratios of ^{18}F-FDG were observed in non-calcified lesions (TBR_{max}=2.2±0.3) compared to mildly calcified lesions (TBR_{max}=1.8±0.4) (p<0.05) and severely calcified lesions (TBR_{max}=1.7±0.4) (p<0.05) (Fig.2), while no significant differences were found between the two groups of calcified lesions (p=0.28).

For ^{18}F-NaF, significantly enhanced osteogenesis-derived uptake was detected in non-calcified lesions (TBR_{max}=2.6±0.7). Likewise, a lower signal for vascular ^{18}F-NaF uptake (TBR_{max}=2.2±0.6; p<0.05) was detected in mildly calcified lesions, while no significant differences were found between the two groups of calcified lesions (p=0.13) and between non-calcified and severely calcified lesions (TBR_{max}= 2.4±0.8; p=0.39) (Fig.2).

Differential changes in osteogenesis, macrophage metabolism, and plaque calcification over time

In the plaque progression study of the 19 patients who were scanned twice (98 lesions), the mean calcium density increased from 580 ± 320 HU (baseline) to 657 ± 328 HU (follow-up) (p=0.07) (Fig.3). At the same time, plaque osteogenic activity, as measured by ^{18}F-NaF uptake

ratios (mean TBR_{max}), significantly increased from 2.5±0.8 (baseline) to 2.8±0.7 (follow-up) ($p<0.05$). In contrast, there was a non-significant trend of decreasing inflammatory activity, as determined by the mean TBR_{max} of ^{18}F-FDG (from 1.9 ± 0.8 at baseline to 1.7±0.4 at follow-up; p=0.25) (Fig.3). Representative ^{18}F-FDG and ^{18}F-NaF PET/CT images of patients who presented with different types of lesions are presented in Figure 4.

Comprehensive group assessments were performed based on the detected changes of both tracers between baseline and follow-up. There were 63% of all lesions that showed concordant changes from baseline to follow-up. Specifically, inflammation and osteogenesis progressed concordantly in 80% of non-calcified (86%) and mildly calcified lesions (81%); however, only 47% of severely calcified lesions exhibited coincident development during plaque progression (Fig.5).

Anti-myeloma medical therapy

Potential interaction with anti-tumor medication was investigated in the 19 patients who got both baseline and follow-up scans with the two tracers: 8 patients (42%) got zoledronic acid and 4 patients (21%) denosumab. In the zoledronic acid group, for ^{18}F-NaF TBR values increased ($TBR_{baseline}$= 2.6 ± 0.8 vs $TBR_{follow-up}$= 2.9 ± 0.7; $p<0.05$), while TBR values for ^{18}F-FDG decreased, which, however, did not reach statistical significane ($TBR_{baseline}$= 2.0 ± 0.9 vs $TBR_{follow-up}$= 1.8 ± 0.4; p=0.13). In the group of denosumab treated paitents, for ^{18}F-NaF TBR values also increased ($TBR_{baseline}$= 2.1 ± 0.8 vs $TBR_{follow-up}$= 2.8 ± 0.6; $p<0.01$), while for ^{18}F-FDG, TBR values remained stable ($TBR_{baseline}$= 1.5 ± 0.4 vs $TBR_{follow-up}$= 1.6 ± 0.3; p=0.64). In the 7 patients without zoledronic acid or denosumab treatment, TBR values remained stable for both tracers (^{18}F-NaF: $TBR_{baseline}$= 2.7 ± 0.9 vs $TBR_{follow-up}$= 2.8 ± 0.8; p=0.61; ^{18}F-FDG: $TBR_{baseline}$= 1.8 ± 0.4 vs $TBR_{follow-up}$= 1.8 ± 0.4; p=0.39).

DISCUSSION

This study investigated the interplay between inflammatory activity and osteogenesis as determined by ^{18}F-FDG and ^{18}F-NaF in atherosclerotic lesions with different degrees of calcification as determined by CT. At the molecular view, hydroxyapatite emerges intensively on the surface of crystallization, fluoride ions interact with the hydroxyapatite by ion exchange with hydroxyl groups, and the uptake of ^{18}F-NaF directly reflects osteogenic activity (*13*). This process is dependent on the density of hydroxyapatite, as well as the exposed surface of calcification in the vasculature. The Agatston score is a semi-quantitative method to calculate the extent of coronary artery calcification, and thresholds of 130 HU and 400 HU are empirically set to define the presence of calcification and severe calcification (*17,22*). Thus, in order to evaluate the arterial calcium extent in the present study, we used a kindred semiquantitative evaluation system, which considered calcium density, to classify groups with different calcification severity (Table 2).

In the present study, higher TBR_{max} values were calculated for ^{18}F-NaF PET as compared to ^{18}F-FDG PET for the same lesions at baseline, which is in accordance with a previous study by Derlin et al. (*23*). In the group assessment, increased uptake of ^{18}F-NaF, an indicator of activated/enhanced osteogenesis, was detected in early atherosclerotic lesions with an undetectable calcium composition and in advanced calcified lesions (Fig 2). These findings are in agreement with previously published research, which demonstrated osteogenic activity at the early atherosclerotic stage, where mineralization is stimulated by macrophage infiltration/activation, as well as at later activated stages, where calcification is induced by both vascular apoptosis and continued macrophage activation (*13,24*). In other words, a high macrophage burden and dense vascular calcification might occur at different-stage calcified segments. In early erosive plaques, inflammatory mediators and elevated lipid content within atherosclerotic lesions induces osteogenic differentiation from immune cells and smooth muscle cells (*25*); during the subsequent later progression of disease, continuous macrophage infiltration precedes osteogenic activity and increased mineralization, where apoptosis of lipid-laden macrophages induces calcium deposition in smooth muscle cells (*26*). Moreover, in late

atherosclerotic plaques, continued development of vascular inflammation might also induce osteogenesis, and drive the plaque to be rupture-risk (*13*).

In the present study, we observed increased vascular osteogenesis and subsequent progressive calcification, compared to reduced inflammation, as detected by ^{18}F-NaF and ^{18}F-FDG PET/CT (Fig.3). In sub-group analyses, non-calcified and mildly calcified lesions during the relatively early progression of atherosclerotic calcification revealed that the majority of lesions proceed in a manner consistent with osteogenic and inflammatory processes. However, there is a discordant regulation of these two processes during the development of the majority of advanced calcified lesions (Fig.5). This also suggests that early atherosclerotic osteogenesis is determined by macrophage accumulation and further intensive progression of arterial calcification might be associated with reduced inflammation. In a novel view, the association between biomechanical stress and plaque pathophysiology describes that calcification more likely occurs at the fibrous cap of plaques, leading to an increased risk of plaque ruptures (*27*).

There was no increased uptake of ^{18}F-NaF in severely calcified lesions and the ^{18}F-NaF uptake did not correlate well with the CT calcium density. This could be explained by the fact, that ^{18}F-NaF uptake is closely associated with onsite hydroxyapatite density, which is deposited on the crystal surface and, thus, does not necessarily reflect the overall calcium density of lesions. Furthermore, vascular calcification presents a different pathophysiology and structure in different arteries according to the hemodynamics and shear stress. Aikawa et al. reported increased osteogenic activity accompanied by an intensive macrophage burden at arterial sites with the greatest amount of mechanical stress (*24*). They also demonstrated that inflammation and osteogenesis evolved in close proximity and overlapped at border regions, and suggested that plaque ruptures might occur in these adjacent areas. These overlapping sites with high mechanical stress might induce an acute pro-inflammatory response, and thus, the subsequent enhanced osteogenesis, which suggested that an increased ^{18}F-NaF uptake at a specific anatomic site serves as a surrogate marker for activated atherosclerotic calcification, not intact calcification. Another reason for the underestimation of ^{18}F-NaF uptake could be the occurrence of partial

volume effects in small, calcified lesions. Dynamic attachment of tracers under distinct flow conditions and the active formation volume of hydroxyapatite crystal can also affect the uptake ratios of ^{18}F-NaF.

Several lines of evidence have suggested that arterial calcification shares features with bone, because the arterial calcified metabolism is indistinguishable from bone lesions, and the arterial osteogenesis shows similarities to new bone formation and development (*7,9*). Bone remodeling consists of the resorption of aged bone components and new bone formation (*28*). We presumed that the components of calcium salts change dynamically during bone progression. Thus, we also inferred that osteogenesis-related calcium salt, hydroxyapatite, may vary on the surface of mineralization during calcification development.

^{18}F-NaF and ^{18}F-FDG PET/CT might provide distinct insights into atherosclerosis progression by providing information on ongoing osteogenesis and inflammation in different-phases of atherosclerosis independently. On the other hand, coronary ^{18}F-FDG uptake is frequently obscured by physiological myocardial uptake, so that ^{18}F-NaF is increasingly used for coronary artery imaging, where increased osteogenesis was recently demonstrated to be associated with cardiac events during follow-up (*13*). While both tracers, ^{18}F-NaF and ^{18}F-FDG, have their strengths and limitations in the evaluation of inflammatory atherosclerosis, the combination of both together with morphological allocation and/or characterization by CT or MRI could improve diagnostic and particularly prognostic accuracy.

We also observed significantly increased ^{18}F-NaF uptake ratios over time with anti-tumor medication of zoledronic acid and denosumab in myeloma patients. Zoledronic acid closely resembles pyrophosphate compounds and inhibits hydroxyapatite breakdown, thereby effectively suppressing bone resorption (*29*). Denosumab is able to slow down bone resorption by interaction with osteoclast cells and enables formation of the bone component (*30,31*). However, due to the relatively low number of patients investigated, the influence of these anti-tumor drugs on atherosclerosis progression and particularly on calcification development remains unclear. Nevertheless, this study might provide a flexible method to assess the effectiveness of anti-plaque

medical therapy in the context of prospective clinical trials.

Limitations of this retrospective analysis must be considered. Firstly, no histological analyses were available as a reference; however, it was previously shown that specific ^{18}F-NaF uptake co-localized with active calcification in histology as well as macrophage infiltration, apoptosis, and necrosis. Secondly, pure non-calcified plaques are difficult to identify on non-contrast CT scans, so that this type of plaques may have been underrepresented. Thirdly, we cannot exclude the influence of anticancer medical therapies or the hormone response of myeloma. Especially for the patients who take immune-modulatory drugs, such as lenalidomid, this interference between drugs and tracer uptake might influence the accuracy and reproducibility of results. It is clear from our data, that further, prospective, methodological studies with larger sample sizes are required to address the prognostic value of ^{18}F-NaF focal uptake and the association between atherosclerotic inflammation and osteogenesis.

CONCLUSION:

Both ^{18}F-FDG and ^{18}F-NaF PET exhibited distinct accumulation during the progression of calcified plaques, but reflect different pathophysiologic processes within atherosclerosis. Therefore, the combination of ^{18}F-NaF and ^{18}F-FDG PET imaging might potentially improve noninvasive identification and characterization of vulnerable plaques.

ACKNOWLEDGMENTS

The authors wish to thank the team of technologists for their constant helpfulness and patient management as well as their engagement in ^{18}F-FDG radiotracer synthesis. Furthermore, Andreas Krcal is acknowledged for his help with ^{18}F-NaF radiopreparations.

REFERENCES

1. Finn AV, Nakano M, Narula J, Kolodgie FD, Virmani R. Concept of vulnerable/unstable plaque. *Arterioscler Thromb Vasc Biol.* 2010;30:1282-1292.

2. Tarkin JM, Joshi FR, Rudd JH. PET imaging of inflammation in atherosclerosis. *Nat Rev Cardiol.* 2014;11:443-457.

3. Robbins CS, Hilgendorf I, Weber GF, et al. Local proliferation dominates lesional macrophage accumulation in atherosclerosis. *Nat Med.* 2013;19:1166-1172.

4. Demer LL, Tintut Y. Vascular calcification: pathobiology of a multifaceted disease. *Circulation.* 2008;117:2938-2948.

5. New SE, Aikawa E. Molecular imaging insights into early inflammatory stages of arterial and aortic valve calcification. *Circ Res.* 2011;108:1381-1391.

6. Ehara S, Kobayashi Y, Yoshiyama M, et al. Spotty calcification typifies the culprit plaque in patients with acute myocardial infarction: an intravascular ultrasound study. *Circulation.* 2004;110:3424-3429.

7. Doherty TM, Asotra K, Fitzpatrick LA, et al. Calcification in atherosclerosis: bone biology and chronic inflammation at the arterial crossroads. *Proc Natl Acad Sci U S A.* 2003;100:11201-11206.

8. Shemesh J, Henschke CI, Shaham D, et al. Ordinal scoring of coronary artery calcifications on low-dose CT scans of the chest is predictive of death from cardiovascular disease. *Radiology.* 2010;257:541-548.

9. Hunt JL, Fairman R, Mitchell ME, et al. Bone formation in carotid plaques: a clinicopathological study. *Stroke.* 2002;33:1214-1219.

10. Derlin T, Richter U, Bannas P, et al. Feasibility of 18F-sodium fluoride PET/CT for imaging of atherosclerotic plaque. *J Nucl Med.* 2010;51:862-865.

11. Irkle A, Vesey AT, Lewis DY, et al. Identifying active vascular microcalcification by (18)F-sodium fluoride positron emission tomography. *Nat Commun.* 2015;6:7495.

12. Dweck MR, Chow MW, Joshi NV, et al. Coronary arterial 18F-sodium fluoride uptake: a novel marker of plaque biology. *J Am Coll Cardiol.* 2012;59:1539-1548.

13. Joshi NV, Vesey AT, Williams MC, et al. 18F-fluoride positron emission tomography for identification of ruptured and high-risk coronary atherosclerotic plaques: a prospective clinical trial. *Lancet.* 2014;383:705-713.

14. Shanahan CM. Inflammation ushers in calcification: a cycle of damage and protection? *Circulation.* 2007;116:2782-2785.

15. Tintut Y, Patel J, Territo M, Saini T, Parhami F, Demer LL. Monocyte/macrophage regulation of vascular calcification in vitro. *Circulation.* 2002;105:650-655.

16. Panin VY, Kehren F, Michel C, Casey M. Fully 3-D PET reconstruction with system matrix derived from point source measurements. *IEEE Trans Med Imaging.* 2006;25:907-921.

17. Agatston AS, Janowitz WR, Hildner FJ, Zusmer NR, Viamonte M, Jr., Detrano R. Quantification of coronary artery calcium using ultrafast computed tomography. *J Am Coll Cardiol.* 1990;15:827-832.

18. Li X, Samnick S, Lapa C, et al. 68Ga-DOTATATE PET/CT for the detection of inflammation of large arteries: correlation with18F-FDG, calcium burden and risk factors. *EJNMMI Res.* 2012;2:52.

19. Rominger A, Saam T, Wolpers S, et al. 18F-FDG PET/CT identifies patients at risk for future vascular events in an otherwise asymptomatic cohort with neoplastic disease. *J Nucl Med.* 2009;50:1611-1620.

20. Emami H, Vucic E, Subramanian S, et al. The effect of BMS-582949, a P38 mitogen-activated protein kinase (P38 MAPK) inhibitor on arterial inflammation: a multicenter FDG-PET trial. *Atherosclerosis.* 2015;240:490-496.

21. Elkhawad M, Rudd JH, Sarov-Blat L, et al. Effects of p38 mitogen-activated protein kinase inhibition on vascular and systemic inflammation in patients with atherosclerosis. *JACC Cardiovasc Imaging.* 2012;5:911-922.

22. van der Bijl N, Joemai RM, Geleijns J, et al. Assessment of Agatston coronary artery calcium score using contrast-enhanced CT coronary angiography. *AJR Am J Roentgenol.* 2010;195:1299-1305.

23. Derlin T, Toth Z, Papp L, et al. Correlation of inflammation assessed by 18F-FDG PET, active mineral deposition assessed by 18F-fluoride PET, and vascular calcification in atherosclerotic plaque: a dual-tracer PET/CT study. *J Nucl Med.* 2011;52:1020-1027.

24. Aikawa E, Nahrendorf M, Figueiredo JL, et al. Osteogenesis associates with inflammation in early-stage atherosclerosis evaluated by molecular imaging in vivo. *Circulation.* 2007;116:2841-2850.

25. New SE, Goettsch C, Aikawa M, et al. Macrophage-derived matrix vesicles: an alternative novel mechanism for microcalcification in atherosclerotic plaques. *Circ Res.* 2013;113:72-77.

26. Proudfoot D, Skepper JN, Hegyi L, Bennett MR, Shanahan CM, Weissberg PL. Apoptosis regulates human vascular calcification in vitro: evidence for initiation of vascular calcification by apoptotic bodies. *Circ Res.* 2000;87:1055-1062.

27. Vengrenyuk Y, Carlier S, Xanthos S, et al. A hypothesis for vulnerable plaque rupture due to stress-induced debonding around cellular microcalcifications in thin fibrous caps. *Proc Natl Acad Sci U S A.* 2006;103:14678-14683.

28. Barrere F, van Blitterswijk CA, de Groot K. Bone regeneration: molecular and cellular interactions with calcium phosphate ceramics. *Int J Nanomedicine.* 2006;1:317-332.

29. Fleisch H. Bisphosphonates: mechanisms of action. *Endocr Rev.* 1998;19:80-100.

30. Boyle WJ, Simonet WS, Lacey DL. Osteoclast differentiation and activation. *Nature.* 2003;423:337-342.

31. McClung MR, Lewiecki EM, Cohen SB, et al. Denosumab in postmenopausal women with low bone mineral density. *N Engl J Med.* 2006;354:821-831.

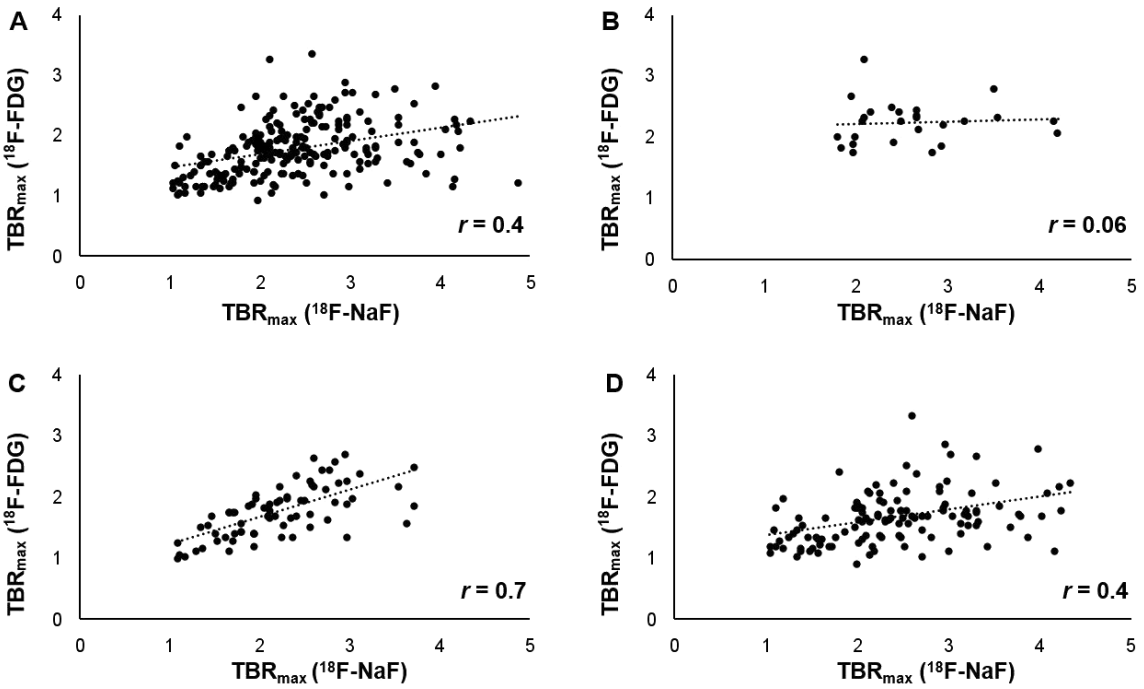

Figure 1. Linear relationship between TBR_{max} values of ^{18}F-NaF and ^{18}F-FDG in (A) all lesions (Pearson r=0.4; p<0.01), in (B) non-calcified lesions (Pearson r=0.06; p=0.76), in (C) mildly calcified lesions (Pearson r=0.7; p<0.01) and in (D) severely calcified lesions (Pearson r=0.4; p<0.01).

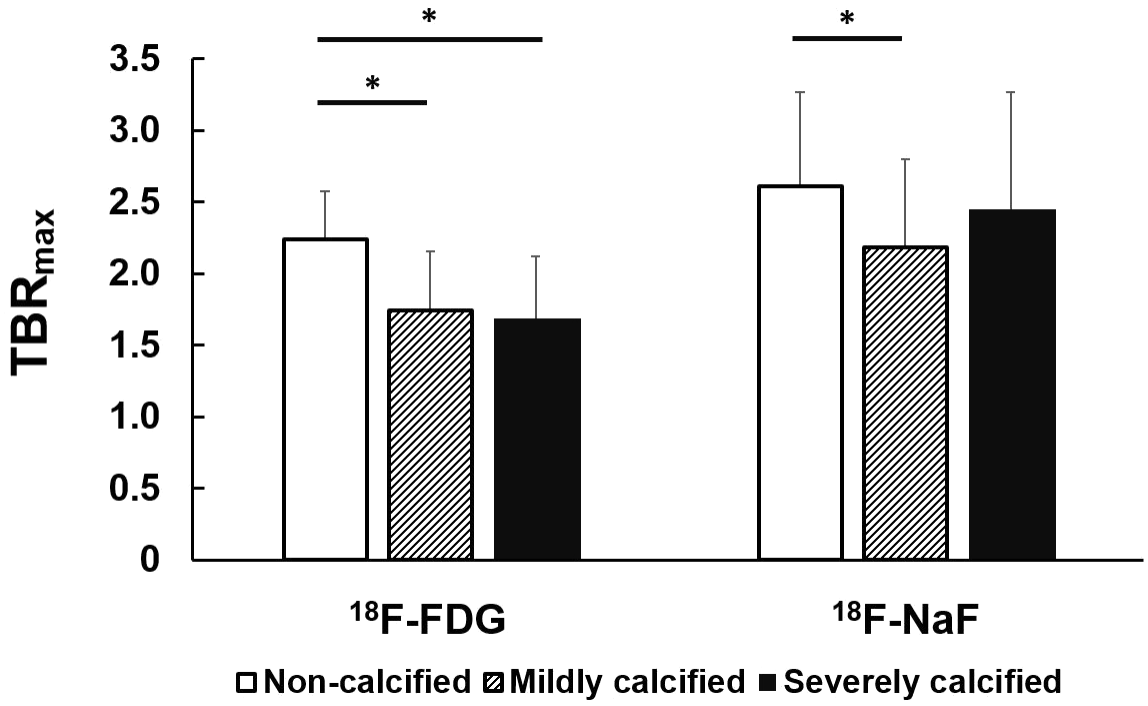

Figure 2. Mean TBR_{max} values of different groups of atherosclerotic lesions according to calcifications. Significant differences ($p<0.05$) are marked with asterisks.

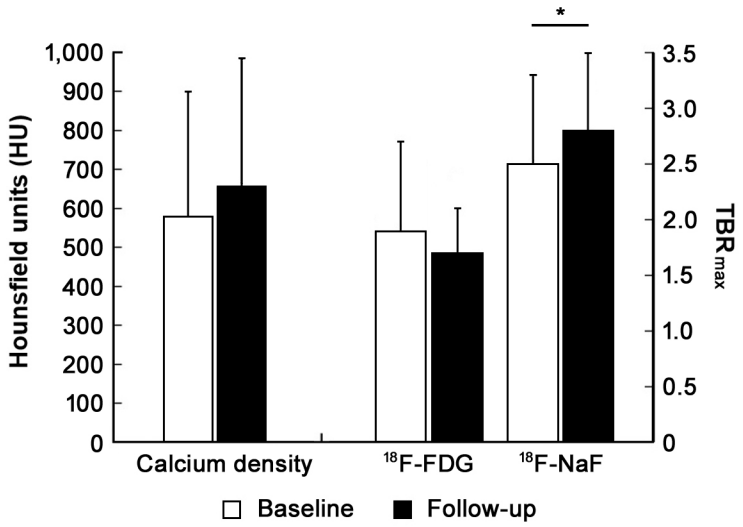

Figure 3. Progression analysis between baseline and follow-up (n=19) for calcium density and uptake ratios of both tracers. Significant changes ($p<0.05$) are marked with asterisks.

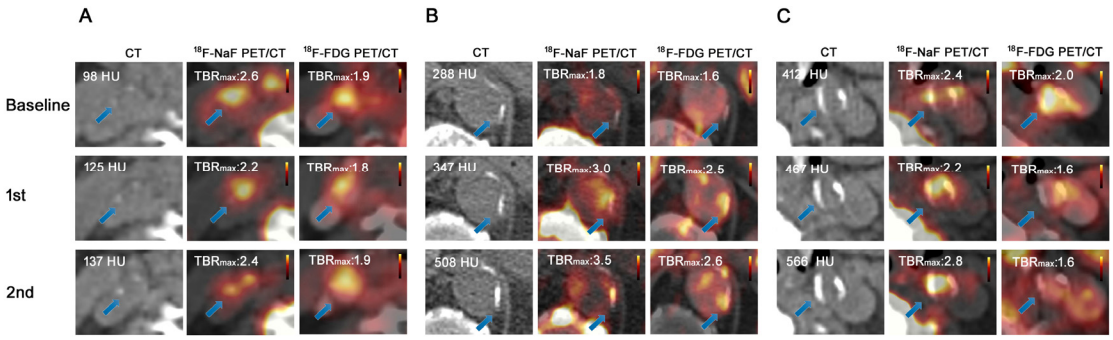

Figure 4. Transaxial ^{18}F-NaF PET/CT images of arterial non-calcified, mildly calcified, and severely calcified lesions from three representative myeloma patients at baseline and at two follow-up scans. (A), in non-calcified lesions, ^{18}F-NaF accumulation in a carotid plaque is co-localized with calcification. Progressive carotid arterial calcium accumulation with enhanced ^{18}F-NaF uptake and subdued ^{18}F-FDG uptake was detected. (B), in mildly calcified lesions, following arterial calcium progression, ^{18}F-NaF uptake progressed intensively, with subdued ^{18}F-FDG uptake ($TBR_{max\_baseline}$=1.6 vs $TBR_{max\_1st\ follow\text{-}up}$=2.5, $TBR_{max\_2nd\ follow\text{-}up}$=2.6) from baseline to follow-up scans. (C), dense calcium composition presented in severely calcified lesions, whereas the progressive ^{18}F-NaF focal uptake ratio was coupled with regression of ^{18}F-FDG uptake during plaque progression. Arrows indicate calcified lesions.

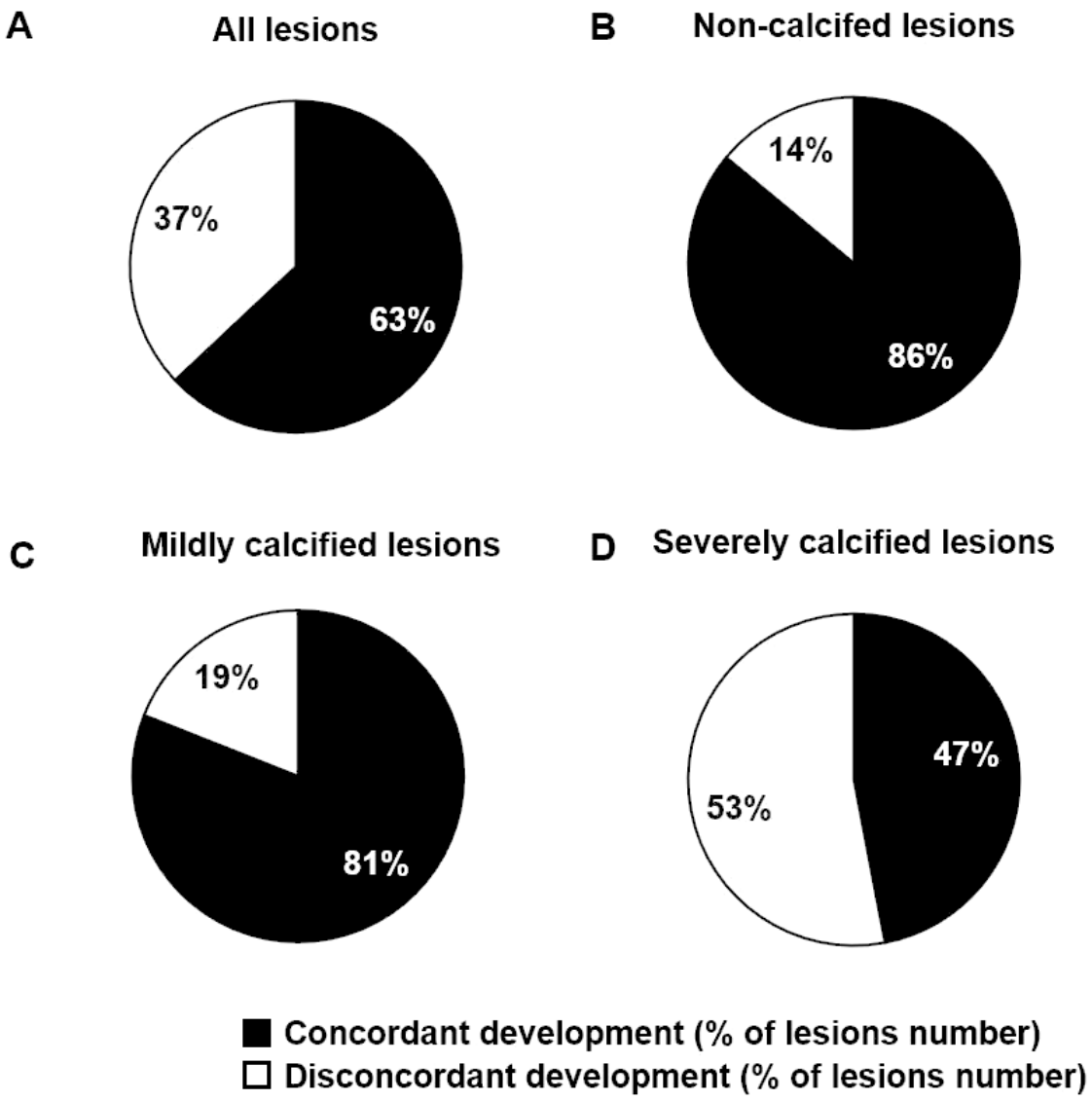

Figure 5. Concomitant development of inflammation and osteogenesis during disease progression. (A), progression or regression developed concordantly in 63% of of all lesions. (B), the majority of both early non-calcified (86%) and (C), mildly calcified lesions (81%) showed concordant changes. (D), only half of the severely calcified lesions (47%) evolved in a manner consistent with vascular inflammation and osteogenesis progression. These results suggested that relatively early atherosclerotic osteogenesis is determined by macrophage accumulation and further intensive arterial osteogenesis might be associated with retardation of inflammation.

Table 1: Patient Characteristics at Baseline (n=34)

Patients characteristics	
Age(y), mean±SD	68±9
Men, n(%)	26 (76%)
Body-mass index(kg/m^2)	
Risk factors n(%)	
Smoking (ex or current)	8 (24%)
Diabetes	2 (6%)
Hypertension	10 (34%)
Hypercholesterolaemia	2 (6%)
Anti-tumor therapy n(%)	
Radiotherapy	10 (30%)
Immunochemotherapy	21 (62%)
Medication at baseline n(%)	
Zometa (zoledronic acid)	19 (56%)
Xgeva (denosumab)	9 (26%)
Serum biochemistry, mean±SD	
Cholesterol $_{baseline}$ (mg/dl)	198 ± 58
Cholesterol $_{follow\text{-}up}$ (mg/dl)	199 ± 59
C-reactive protein $_{baseline}$ (mg/dl)	0.7 ± 0.7
C-reactive protein $_{follow\text{-}up}$ (mg/dl)	0.7 ± 0.6

Table 2: Criteria for classification of inflammation and osteogenesis development based on changes in ^{18}F-FDG and ^{18}F-NaF uptake.

Stabilized Inflammation/Osteogenesis (TBR_{max}_FDG/ TBR_{max}_NaF)	**Progressive Inflammation/Osteogenesis (TBR_{max}_FDG/ TBR_{max}_NaF)**
TBR_{max} (Baseline) ≤ 1.6/1.8 TBR_{max} (Follow-up) ≤ 1.6/1.8 Increasing TBR_{max} ≤ 30% & Decreasing TBR_{max}	TBR_{max} (Baseline) ≤ 1.6/1.8 TBR_{max} (Follow-up) ≤ 1.6/1.8 Increasing TBR_{max} ≥ 30%
TBR_{max} (Baseline) ≥ 1.6/1.8 TBR_{max} (Follow-up) ≥ 1.6/1.8 Decreasing TBR_{max} ≥ 30%	TBR_{max} (Baseline) ≥ 1.6/1.8 TBR_{max} (Follow-up) ≥ 1.6/1.8 Decreasing TBR_{max} ≤ 30% & Increasing TBR_{max}
TBR_{max} (Baseline) ≥1.6/1.8 TBR_{max} (Follow-up) ≤1.6/1.8 Decreasing TBR_{max} ≥ 10%	TBR_{max} (Baseline) ≥1.6/1.8 TBR_{max} (Follow-up) ≤1.6/1.8 Decreasing TBR_{max} ≤ 10%
TBR_{max} (Baseline) ≤ 1.6/1.8 TBR_{max} (Follow-up) ≥ 1.6/1.8 Increasing TBR_{max} ≤ 10%	TBR_{max} (Baseline) ≤ 1.6/1.8 TBR_{max} (Follow-up) ≥ 1.6/1.8 Increasing TBR_{max} ≤ 10%